

Functional Plasmonic Nanocircuits with Low Insertion and Propagation Losses

Arian Kriesch,^{*,†,‡} Stanley P. Burgos,[‡] Daniel Ploss,[†] Hannes Pfeifer,[†] Harry A. Atwater,[‡] and Ulf Peschel[†]

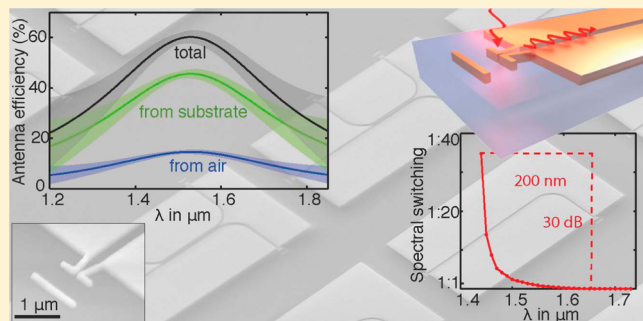
[†]Institute of Optics, Information and Photonics, Erlangen Graduate School in Advanced Optical Technologies, Friedrich-Alexander-University Erlangen-Nuremberg (FAU) and Max Planck Institute for the Science of Light, 91058 Erlangen, Germany

[‡]Kavli Nanoscience Institute, California Institute of Technology, Pasadena, California 91125, United States

Supporting Information

ABSTRACT: We experimentally demonstrate plasmonic nanocircuits operating as subdiffraction directional couplers optically excited with high efficiency from free-space using optical Yagi-Uda style antennas at $\lambda_0 = 1550$ nm. The optical Yagi-Uda style antennas are designed to feed channel plasmon waveguides with high efficiency (45% in coupling, 60% total emission), narrow angular directivity ($<40^\circ$), and low insertion loss. SPP channel waveguides exhibit propagation lengths as large as $34 \mu\text{m}$ with adiabatically tuned confinement and are integrated with ultracompact ($5 \times 10 \mu\text{m}^2$), highly dispersive directional couplers, which enable 30 dB discrimination over $\Delta\lambda = 200$ nm with only 0.3 dB device loss.

KEYWORDS: SPP, circuit, antenna, waveguide, directional coupler, Yagi-Uda



Surface plasmon polariton (SPP) waveguides are uniquely advantaged by their high confinement, allowing for subwavelength integration. This is a requirement for integrating optics with a footprint size that is comparable with electronic circuits, thus enabling plasmonic-electronic hybrid integration, a path that has been repeatedly highlighted as a future key application of plasmonics.^{1–4} However, high confinement in plasmonics usually increases loss due to the larger field overlaps with the metal. The second major obstacle to deep subwavelength plasmonics is high insertion loss due to the limited modal field overlap of less-confined waveguide schemes like Si integrated photonics^{5,6} or optical fibers,⁷ thus intrinsically limiting the performance of hybrid dielectric-plasmonic circuits.⁸

Here, we illustrate how in-circuit-loss can be mitigated by restricting strong optical confinement only to components where it is absolutely essential (Figure 1c), and how insertion-loss can be addressed by coupling light into plasmonic nanocircuits via impedance-matched optimized Yagi-Uda⁹ style nanoantennas (Figure 1a,d). Using this platform, we experimentally demonstrate optical directional couplers^{10,11} integrated on a micrometer scale that show unusually strong spectral dispersion, a key prerequisite for integrated wavelength division multiplexers.

To implement these device concepts, we use SPP channel waveguides (also called SPP gap waveguides),^{12,13} which offer maximum confinement¹⁴ in a narrow rectangular gap etched a few hundred nanometers into a metal film. We note that this waveguide geometry does not suffer from optical mode cutoff

when scaled down. By filling the air gap ($n = 1$) in the plasmonic waveguide with the substrate material silica ($n \approx 1.45$) (Figure 1b) we make the modal field distribution more symmetric, therefore eliminating an upper modal cutoff that otherwise prohibits larger waveguide channel widths (>80 nm for usual Au channel waveguides), therefore limiting the propagation length to below $10 \mu\text{m}$. Wherever possible, the connections from one functional plasmonic unit to the next must be bridged with low loss plasmonic waveguides. As the waveguide mode is basically maintained for different channel widths, easy to fabricate adiabatic waveguide tapers can form the transition from highly confining to low loss sections. We experimentally demonstrate that the investigated circuits achieve a propagation length of $L_{\text{p/e}} = 34 \mu\text{m}$, while they are still subwavelength with a waveguide gap width of 300 nm and that they have an effective refractive index of $n_{\text{eff}} \approx 1.54$ at $\lambda_0 = 1550$ nm with low dispersion.

To reduce insertion loss, each presented nanoplasmonic circuit utilizes at least two connected Yagi-Uda antennas to enhance coupling efficiency from a focused laser beam and to achieve narrow directivity (Figure 1a,d). We measured the antenna and waveguide properties spectrally and derive their fundamental properties: efficiency (45% in coupling, 60% total emission), directivity ($<40^\circ$), and spectral dispersion.

Received: July 13, 2013

Revised: August 14, 2013

Published: August 20, 2013

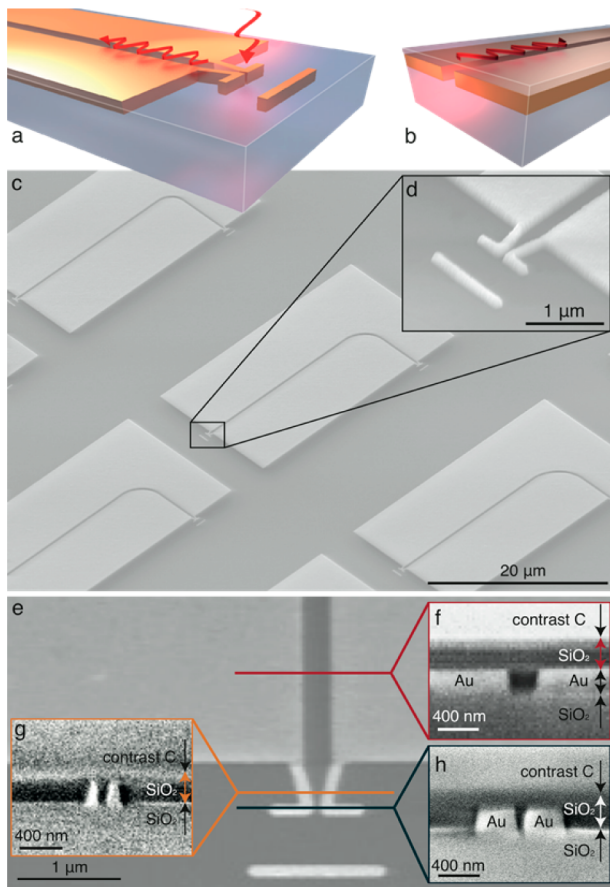


Figure 1. (a) Optical loaded Yagi antennas are optimized to couple a highly focused, linearly polarized laser beam into waveguides (b) that are covered with a cladding layer of spin-on-glass. (c) SEM of an array of multicomponent plasmonic nanocircuits and (d) of a single Yagi antenna. Cross-section cuts with a focused ion beam device (FIB), (f) through the 300 nm wide waveguide, (g) the antenna connector, and (h) the antenna with a minimum feature size of only 80 nm display the sandwich of a substrate layer of silica, the 220 nm thick metal structures and the 320 nm thick cladding layer of spin-on-glass, which completely fills the metal gaps.

For our experiments, embedded SPP nanocircuits (Figures 1c and 6b) were fabricated in a two-step process. A 220 nm thin Au film on a thin 160 μm thick, polished quartz glass substrate was patterned by lift-off with a 100 kV electron beam lithography system. The designed minimum feature size at the antenna gap (Figure 1e,h) was 80 nm. Subsequently, flowable spin-on glass (Filmtronics 400F) was spin-coated and baked to form a dielectric cladding layer. Scanning electron microscope images of device cross sections, cut with a focused ion beam (FIB) at different positions, show that the cladding layer fills all gaps, covers the whole structure without cavities (Figure 1f–h), and forms a smooth surface that is \sim 320 nm higher than the underlying structures. The fabricated circuits consistently deviate less than 15° from perfectly rectangular sidewall angles. To investigate the dependence of the optical properties of each circuit component on design parameters, arrays of circuits were fabricated, while systematically varying waveguide length and bend radii (Figure 1c).

Spectral transmission measurements of each circuit were taken on an optical far-field excitation and imaging setup¹⁵ with a 4 W supercontinuum light source, spectrally filtered to $\lambda = 1200\text{--}1850\text{ nm}$ at 5 nm fwhm with an acousto optical tunable

filter (AOTF) (for sketch and details see Supporting Information). A collimated and linearly polarized laser beam was focused by an objective ($\text{NA} = 0.9$ dry respectively 1.3 oil immersion) to a diffraction-limited spot ($\varnothing < 2\text{ }\mu\text{m}$). The sample was positioned with 5 nm resolution on a stabilized piezo stage to couple maximum power into the optical antennas (Figure 1a,d). The whole circuit was simultaneously imaged with 150 \times or 300 \times magnification through the excitation objective, a polarization filter and NIR imaging optics on an infrared InGaAs CCD camera (Xenics XS, 320 \times 256 pixels). With this setup, the linearly polarized emission from output antennas, turned by 90° with respect to the input antenna (Figure 1c), was imaged with enhanced dynamic range by suppressing the back-reflection from the incident beam with a ratio of up to 10 000. Absolute circuit transmission values were determined by normalizing with the spectral reflectivity of a silica-air interface on the same sample (see Supporting Information for details). With additional Fourier imaging, the polarization dependent angular emission pattern of the antennas was analyzed.

For any application, including probing the circuit properties presented here, light has to be coupled into and out of the guided mode of the plasmonic waveguide with highest possible power conversion efficiency.² Plasmonic antennas are best suited to fulfill this task for exciting channel plasmons from freespace.^{16,17} The concept of optical antennas has already been successfully transferred from well-proven radiofrequency technology to the optical and near-infrared with a resulting antenna size in the micrometer range.^{18–20} Here we apply the macroscopic design concept of Yagi-Uda antennas⁹ in the near-infrared^{21–25} and connect them to feed the plasmonic circuits.

For the investigated antennas, the feed element, an approximately 1 μm long, 100 nm wide, split Au rod, is centrally illuminated with a focused laser beam ($\varnothing < 2\text{ }\mu\text{m}$) that is polarized parallel to the antenna arms (Figure 1a,d). This element is driven at its resonance frequency and feeds the 300 nm wide SPP channel waveguide. An additional nonresonant Yagi-reflector element is placed in a distance of 600 nm to the feed element to constructively reflect the electromagnetic field back into the waveguide, thus enhancing the in-coupling efficiency.

Our whole design was developed using an iterative particle-swarm-optimization algorithm based on full 3D FDTD simulations while taking into account the limitations of fabrication and real optical material parameters as determined with ellipsometry. As it was found that in-coupling efficiency increases with decreasing size of the antenna gap,²¹ we limited the antenna gap dimension to 80 nm based on fabrication limitations. A taper was added to connect the antenna with a 300 nm wide low-loss waveguide to minimize impedance mismatch and back reflections.

To simplify the experimental analysis of our circuits we attributed lumped properties to each element (Figure 2a).¹ The antennas were assigned a characteristic spectral transmission $T_{\text{ant}}(\lambda) = P_{\text{wg}}(\lambda)/P_{\text{freespace}}(\lambda)$ that represents the ratio of power, which is converted into the waveguide mode for a specific wavelength, a spectral absorption $A_{\text{ant}}(\lambda)$ due to ohmic losses and a reflectivity $R_{\text{ant}}(\lambda)$ at the antenna-waveguide connection caused by residual impedance mismatch.^{1,17} For the waveguides, we assigned a length-dependent transmission $T_{\text{wg}}(\lambda, L) = 1 \text{ e}^{-L/L_0}$ that is quantified in terms of the propagation length L_0 of their supported SPPs. Hence, L_0 is separated by multiple measurements over a systematic variation of the waveguide

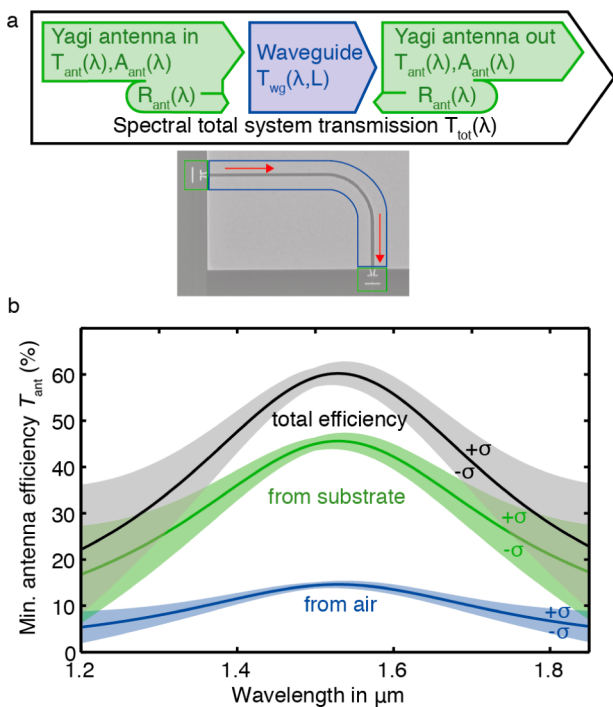


Figure 2. (a) The plasmonic circuits are analyzed as a sequence of black boxes, each with a characteristic, spectral transmission $T(\lambda)$, absorption loss $A(\lambda)$, and reflection coefficient $R(\lambda)$ toward the waveguide. (b) Experimentally determined lower bound for the spectral efficiency of the Yagi antennas $T_{\text{ant}}(\lambda)$ reaching a spectral peak value of 60% of intensity to couple the bound mode inside the waveguide out into air (15%) and silica (45%), respectively, from a focused beam into the waveguide. The antenna efficiency was determined by fitting measured data with a Lorentzian line shape and separating loss effects. The shaded areas indicate $\pm\sigma$ error bands.

length L . In applying this model to our experiments, we further assume that in- and out-coupling antennas had similar, inversion-invariant properties. This is a reasonable approximation as we inject and extract light using the same objective. Hence, the total system transmission is given by $T_{\text{tot}}(\lambda) = T_{\text{ant}1}(\lambda)T_{\text{wg}}(\lambda)T_{\text{ant}2}(\lambda) = T_{\text{ant}}(\lambda)^2T_{\text{wg}}(\lambda)$.

We experimentally measured the spectral system transmission $T_{\text{tot}}(\lambda)$ in the range of $\lambda = 1200 - 1850 \text{ nm}$ in steps of 5 nm, coupling in and out of the circuit from air or through the silica substrate. An ensemble of 20 (5×5) different plasmonic nanocircuits was characterized (Figure 1c), repeated on 4 different samples with the same fabrication settings. Each parameter variation ensemble contained circuits with different total waveguide lengths ($L = 12.28 - 42.28 \mu\text{m}$) and different radii ($R = 1 - 4 \mu\text{m}$) for the 90° bend that turns the waveguide mode polarization for the emitting antenna. A systematic analysis of the bend loss over radius demonstrated that bends with $R = 3, 4 \mu\text{m}$ offer negligible additional loss compared to the linear waveguide propagation loss, which is comprehensible since the modal effective wavelength difference for those radii is negligible compared to straight waveguides. Hence, we focused our analysis to circuits with a $3 \mu\text{m}$ bend radius.

On the basis of this finding, we fitted the transmissions of the circuits with an iterative two-dimensional least-squares fit over the independent variables wavelength and waveguide length. The antenna transmission was modeled assuming a Lorentzian spectral broadening response, $T_{\text{ant}} = T_{\text{ant}}^{\max}/[1 + ((\lambda - \lambda_0)/\gamma)^2]$. Under the assumption that dispersive effects of the in- and outcoupling are solely caused by the antenna resonance, we find that the peak wavelength λ_0 and line width γ are independent of the excitation, whereas the maximum antenna efficiency T_{ant}^{\max} is higher for excitation from and emission into the substrate than into air due to the refractive index asymmetry of the structure, $n_{\text{substrate}} \approx 1.44 > n_{\text{air}} = 1$.

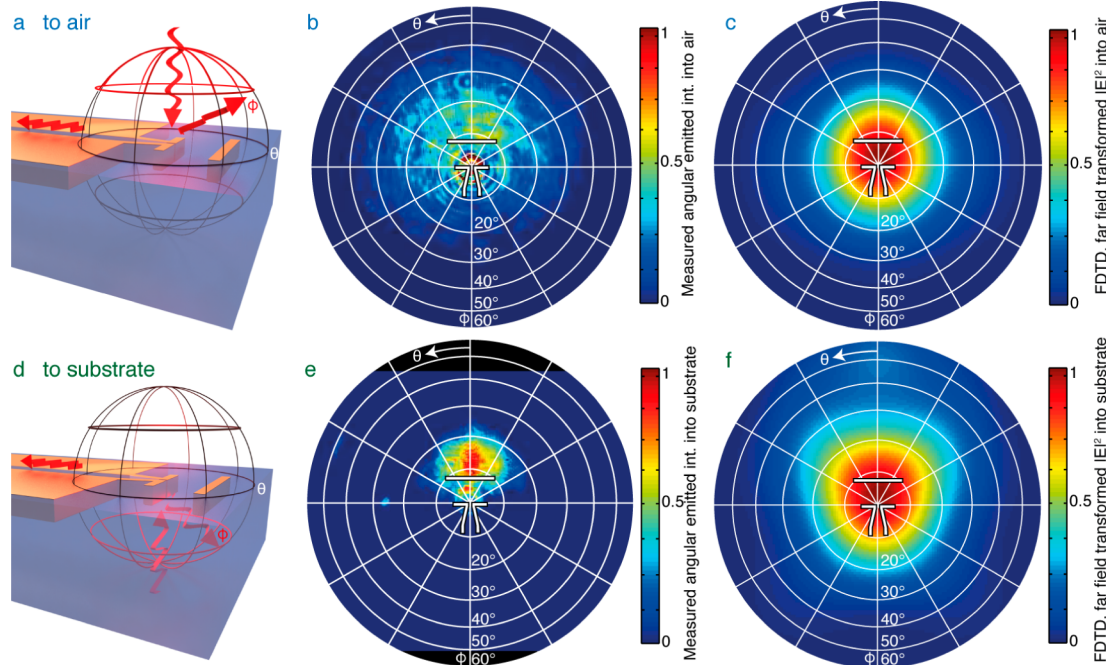


Figure 3. A narrow and strongly linear polarized angular emission directionality of the Yagi antenna at $\lambda = 1550 \text{ nm}$ (a–c) into air and (d–f) into the silica substrate was measured experimentally by Fourier plane imaging of the antenna emission during excitation with (b) an objective of NA = 0.9 and (e) an immersion objective of NA = 1.3. The maximum azimuthal emission cone of 30° is in accordance with the 3D FDTD simulation of the same structure into (c) air and (f) silica.

From this fit the spectral propagation length $L_0(\lambda)$ (Figure 5a, blue curve) and the spectral antenna transmission $T_{\text{ant}}(\lambda)$ were determined over all measurements and circuits (few circuits with obvious fabrication errors were excluded from the evaluation). The fit error (standard deviation σ), therefore includes statistical errors of both the measurement and fabrication (Figure 2b). The determined antenna efficiency is a lower limit, as we might not have eliminated all possible sources of losses in the circuit. The antenna transmission peaks at $\lambda_{\text{max}} = 1530 \text{ nm}$ with a spectral width of $\gamma = 244 \text{ nm}$, corresponding to a fwhm = 488 nm. The spectral peak efficiency of the antennas is $T_{\text{ant,air}}^{\text{max}} = 15 \pm 1\%$ from air and $T_{\text{ant,substr}}^{\text{max}} = 45 \pm 2\%$ from the substrate with minimum statistical error around the peak and increasing error toward the measurement limits of $\lambda = 1200 \text{ nm}$ and $\lambda = 1850 \text{ nm}$, where the absolute circuit transmission and the InGaAs camera efficiency decrease.

Keeping the initial assumption that the antenna properties obey optical inversion symmetry, the total antenna efficiency, giving the total emission into air and silica, can be spectrally summated to be $T_{\text{ant,tot}}^{\text{max}} = 60 \pm 3\%$, the highest power transmission for a waveguide loaded optical antenna, reported to date.

Validity of the applied transmission analysis is based on the hypothesis that the objective collects all light that is emitted from the Yagi antennas and that a good overlap of the focused exciting beam and the angular emission directionality is achieved. To verify this assumption, the antenna was excited from air (Figure 3a) and from the substrate (Figure 3d), while the far-field emission of the antenna was imaged into the excitation direction (Figures 3b,e) in the Fourier plane and compared to the angular emission spectrum obtained from 3D FDTD simulation with the same geometry parameters and excitation (Figures 3c,f). In experiment and simulation, the antenna emits with strong directionality within a polar angle cone of $\Phi \lesssim 40^\circ$, which is remarkably narrow^{17,23} and completely covered by the NA of our objectives (NA = 0.9 from air and 1.3 immersion from silica). Hence, radiative losses seem to play a minor role in our measurements.

However, the guided field in a waveguide cannot be directly measured in the far-field with the only limited information coming from slight scattering of impurities in strongly overexposed leakage microscopy (see Supporting Information). Therefore aperture near-field scanning optical microscopy (NSOM) was used to image the antennas and waveguides (Figure 4a) directly.

The field distribution of the focused beam at the antenna, as predicted by 3D FDTD simulations (Figure 4c), leads to a distortion of the incident beam in the area between the antenna feed element and the reflector (Figure 4b). No propagating waves are visible along the surface of the sample away from the antenna, demonstrating the efficiency of the Yagi reflector. We note that the evanescent field of the guided mode inside the waveguide is still possible to image through the 320 nm thick cladding layer, which is an advantage for probing the operation of the nanocircuit dynamics.

Embedded SPP channel waveguides feature a characteristic propagation length and effective refractive index. In particular, the latter property is important for potential applications as it determines the phase velocity, but it is usually difficult to measure, as phase information is lost when measuring emitted intensities. From transmission measurements on circuits with short waveguides, we found spectral oscillations on the total

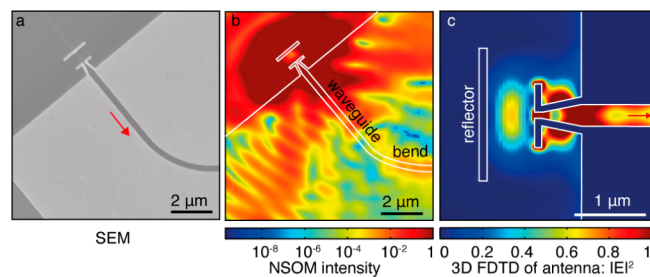


Figure 4. (a) SEM of a Yagi antenna that was illuminated with a highly focused beam through the substrate and (b) scanned with an aperture near-field optical microscope (NSOM) through the 300 nm thin layer of cladding SiO₂. Strong enhancement of the spatial near-field distribution is visible around the antenna and the Yagi reflector. The reflector suppresses emission of the antenna away from the waveguide and couples the electromagnetic wave into the SPP channel waveguide with only slight emission toward the cladding. (c) Electric-field distribution ($|E|^2$) in the structure plane of the optimized antenna geometry from a full 3D FDTD simulation in the same configuration as the measurement.

transmission with maximum amplitude at the antenna resonance, which correspond to Fabry-Pérot resonances, allowing us to probe the mode index of the waveguides.

For the shortest waveguides ($L = 14.28 \mu\text{m}$), the spectral oscillations are very distinct (Figure 5b). The lumped circuit transmission model (Figure 2a) allows us to treat the circuit as a Fabry-Pérot resonator defined by a channel waveguide of length L and mirrors formed by the antennas due to imperfect antenna impedance-matching. This model was fitted to the spectral system transmission, taking the already determined waveguide loss (Figure 5a, blue curve) and the antenna efficiency into account. Hence, the effective refractive index of the waveguide mode (Figure 5a, green curve) was determined to be $n_{\text{eff}} \approx 1.54$ at $\lambda_0 = 1550 \text{ nm}$ with low spectral dispersion, a value that coincides well with the expected guided mode effective index from FDTD calculations.

Simulated modal field distributions (Figure 5a insets) indicate decreasing confinement and increasing field-overlap with the dielectric for longer wavelengths,²⁶ thus explaining the experimentally observed decrease in propagation loss for these wavelengths (Figure 5a, blue curve).

We integrated the developed Yagi antennas and waveguides with optical directional couplers (ODC) in the developed nanoplasmonic circuit platform, demonstrating the functional application of subdiffraction plasmonics as ultrashort coupling length devices. ODCs have been a standard component in macroscopic integrated and fiber optics for several decades.¹¹ They allow for defined, dispersion-engineered transfer of power from one waveguide (bar) to a second waveguide (cross) by evanescent coupling of the field of the guided modes, which can be well described with coupled-mode-theory.¹⁰ The coupling-ratio $I_{\text{cross}}/I_{\text{bar}}$ can be tuned with the length of the coupler. In the investigated nanocircuits, two embedded SPP waveguides run in parallel for up to 12 μm (Figure 6b). The 3D FDTD simulations of the ODC (Figure 6a) clearly show that with thin metal filaments between the two waveguides the investigated geometry features coupling lengths L_c for a first full power transfer from bar to cross down to few micrometers.

Feed (Figure 6b, red) and probe antennas (Figure 6b, green), and an additional fourth antenna for monitoring internal back-reflections (Figure 6b, blue) are connected to the different ports of the ODC. As before, the emission antennas

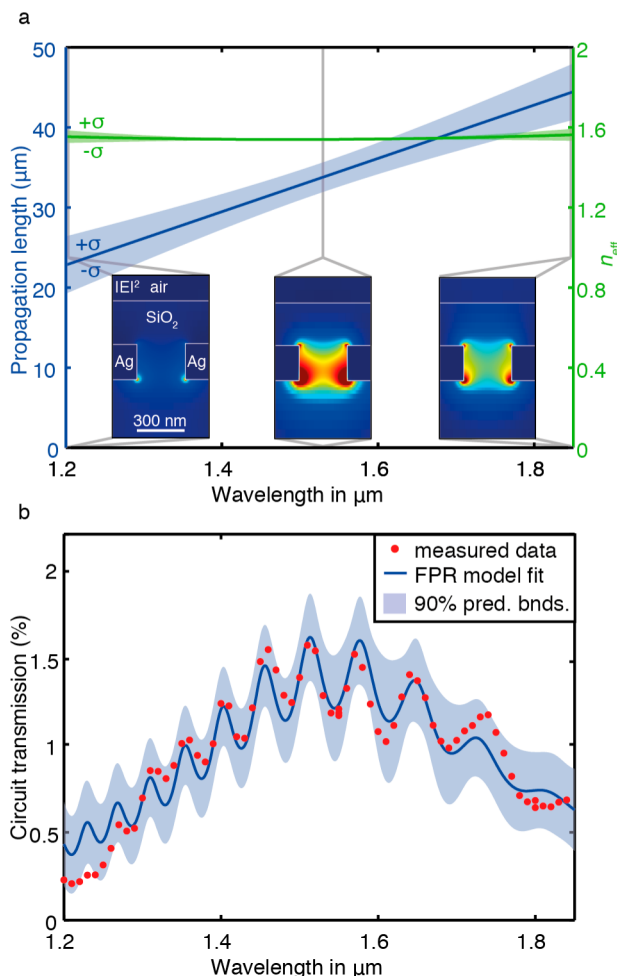


Figure 5. (a) The 300 nm wide and 220 nm deep embedded SPP channel waveguides offer remarkably low loss with a propagation length of P_0/e ($\lambda = 1550$ nm) = 34 μm . Propagation length and dispersion (blue curve) were determined by iterative fitting to the experimental spectral circuit transmission for series of different waveguide lengths. The effective refractive index of the SPP mode was determined as n_{eff} ($\lambda = 1550$ nm) = 1.54 with flat dispersion, by (b) iterative fitting of a Fabry-Pérot oscillator model the experimental spectral transmission (see Figure 3a). The shown pronounced oscillations (red dots) are caused by slight back-reflections of the wave inside the waveguide from the antennas in circuits with 12.28 μm length.

are all turned by 90°, radiating with a linear polarization perpendicular to the excitation antenna. The length of the couplers was varied in an array of optical circuits (Figure 6c) from $L = 0$ –12 μm in 3 μm steps in one direction, while the nominal width of the filament that separates the waveguides was varied from $w = 50$ –90 nm in 10 nm steps in the other. Even the smallest, 50 nm thin metal filaments (aspect ratio 4.4 for a 220 nm metal film) demonstrated good fabrication fidelity over the entire 12 μm length of the longest couplers (Figures 6d,e). To enable smooth transitions, the cross waveguide approaches the bar waveguide in a 90° bend with a radius of $R = 3 \mu\text{m}$, which for the single waveguide circuits showed negligible bend loss. Fabrication was consistently reproducible with four different samples.

As for the basic straight waveguide system, the directional coupler was spectrally probed and modeled with a slightly more elaborate lumped circuit model (Figure 7a) in which the

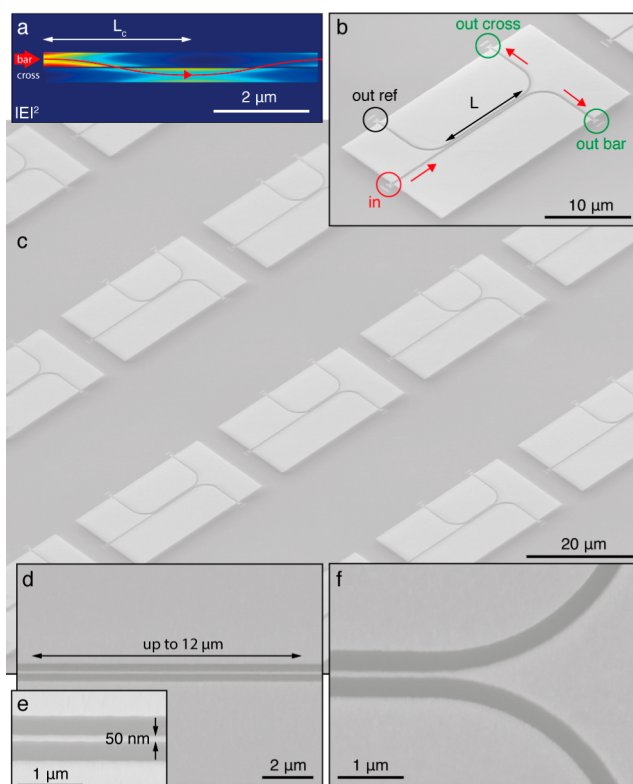


Figure 6. (a) Two embedded SPP channel waveguides in close vicinity exchange energy and form an optical directional coupler (ODC) with a subwavelength length $L_c = 2.46 \mu\text{m}$ for full transfer of the displayed power flow from waveguide bar to cross (in-plane cross section of a 3D FDTD with the experimental geometry). (b) For full spectral characterization of this passive SPP component, it was integrated into a nanocircuit and probed with 4 Yagi antennas, one to couple in (red), two emitting in crossed polarization to observe cross and bar (green), and one to monitor internal reflections (blue). (c) The ODC parameters, length, and waveguide separation were varied systematically. (d,e) The thinnest separation is formed by an only 50 nm wide, 220 nm deep filament of Au, running uniformly over a length of up to 12 μm . (f) At the beginning and the end of the ODC, the waveguides approach with a smooth, adiabatic bend that already causes significant coupling.

previously investigated Yagi antennas are connected to the directional coupler with a characteristic spectral transmission $T_{wg}(\lambda, L)$ and coupling length $L_c(\lambda)$. Each circuit was probed at $\lambda_0 = 1550$ nm, while two clearly distinct emission spots from the cross and bar antenna were separately integrated and the total system transmission was monitored similar as for the single waveguide circuits. (Figure 7e, see Supporting Information for details). We note that the resulting power ratio is intrinsically robust to variations of the coupling efficiency into the circuit as those variations simply lead to a linear scaling of the emission from both monitor antennas.

Coupled mode theory predicts a power exchange between the waveguides in analogy to two weakly coupled damped harmonic oscillators.¹⁰ An iterative least-squares fit of this model was applied to the measured cross- and bar- emission, while being careful to avoid numerical divergences and ensuring equal weighting of all emission ratios (see Supporting Information for details). Following this fit routine, we obtained a reproducible coupling length of only $L_c = 2.46 \pm 0.04 \mu\text{m}$ for the thinnest filament width of 50 nm. This fit, as a second free parameter, determines an additional equivalent length $L_{\text{bend}} =$

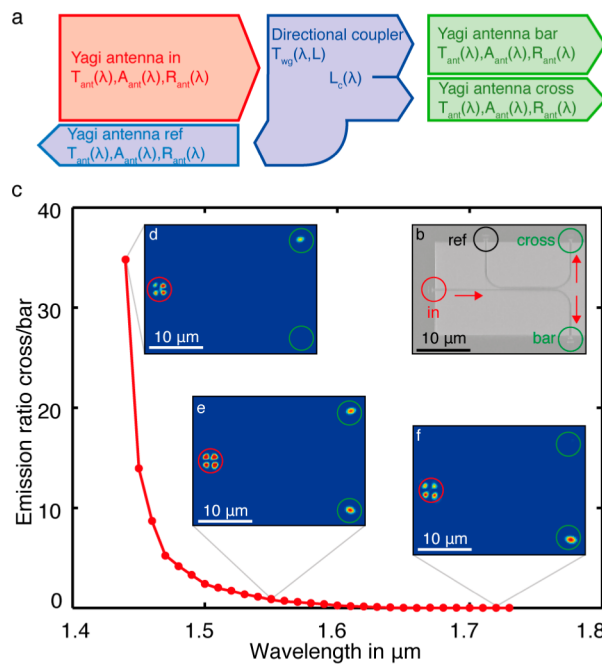


Figure 7. (a) Schematic diagram and (b) SEM of an ultracompact SPP circuit with four Yagi antennas (red in, green out, black reflection reference) and a directional coupler (coupler length $L = 10 \mu\text{m}$), designed for several full coupling cycles at $\lambda = 1550 \text{ nm}$. It shows strong spectral dispersion of the coupling length $L_c(\lambda)$. (c) This leads to full switching of the power from output channel cross to bar (green), clearly visible in the optical emission images for (d) 1440, (e) 1550, and (f) 1720 nm, resulting in a 30 dB wavelength discrimination between 1450 and 1650 nm, while back-reflections (black) are negligible.

$1.7 \pm 0.07 \mu\text{m}$ of the coupler that is caused by the transition into and out of the straight coupling region by 90° bends (Figure 6). Hence, even ODCs with a parallel coupler length of $L = 0 \mu\text{m}$ demonstrated significant coupling of the guided plasmon from the bar waveguide over to the cross waveguide. Furthermore, direct comparison of experimental and FDTD results demonstrate that the fabricated filament widths are effectively a bit smaller than expected, which is reasonable since the metal side-walls are inclined $\sim 15^\circ$ from the vertical, as is evident from SEM cross-sectional images of the fabricated device (Figures 1f–h). Consequently, ODCs simulated with a rectangular filament of 40 nm width (Figure 6a) had the same coupling length as real couplers consisting of 50 nm angled filaments. A complete ODC device can therefore be integrated into an unprecedentedly small area,^{11,27,28} while maintaining reasonably low loss (Figure 5a, blue), therefore achieving a single coupling length system transmission of 0.93, respectively a loss of -0.31 dB .

The dispersion of directional couplers is utilized in many compact wavelength division multiplexing (WDM) systems¹⁰ as it allows for low-loss wavelength division. Probing the spectral transmission of the investigated ODC circuits reveals a pronounced wavelength-dependence.

We characterized different ODCs spectrally in a range of $\lambda_0 = 1250 - 1850 \text{ nm}$. Starting with $\lambda_0 = 1550 \text{ nm}$, the ODCs with a filament width of 70 nm and length of $L = 10 \mu\text{m}$ (Figure 7b) operating with several full coupling lengths demonstrated a well-balanced output with $I_{\text{cross}}/I_{\text{bar}} \approx 1$ (Figure 7e). Then, by sweeping the wavelength we observed full switching between cross (Figure 7d) and bar (Figure 7f) in going from short to

long wavelengths, leading to a 30 dB wavelength discrimination between 1450 and 1650 nm (see Supporting Information for a video demonstrating spectral switching). The whole device features a footprint of only $\sim 5 \times 10 \mu\text{m}^2$ and could easily be stacked to form an arrayed WDM, enabling even more narrow wavelength discrimination within little more space. The size is extremely compact compared to current dielectric integrated WDMs requiring millimeter dimensions.⁶

The strong dispersion of the coupling is dominated by the frequency dependent dielectric constant of the Au as the field-penetration into the thin metallic filament between the waveguide is deep. Thus, inside the ODC the total metal-field overlap is large compared to the single waveguide where the metal-dispersion does not influence the effective index of the mode considerably (Figure 5a, green curve). However, the low dispersion is a desired property for the waveguides as is the high dispersion of the couplers for reducing the effective size of the ODC.

In conclusion, we have demonstrated a highly reproducible design scheme for plasmonic nanocircuitry that combines the high confinement and dispersive properties of plasmonics²⁸ together with the low-loss and high-coupling efficiencies of Yagi-Uda antennas. For the first time, loaded optical Yagi antennas are used to reduce insertion loss and couple light with a high total efficiency of 60% (15% from air, 45% from substrate) into and out of plasmonic nanocircuits. Furthermore, this platform is used to demonstrate the operation of embedded SPP based ODCs with extraordinarily short coupling length. The ODCs feature low transmission loss and compete well with other, for example, Si-integrated circuitry components^{6,27} in terms of coupling-length-overloss ratio while being superior in overall compactness. Distinct spectral switching is observed, thus allowing down-scaling of wavelength division multiplexing from the millimeter to the micrometer range. Additional, we note that other nanoplasmonic circuitry components can easily be transferred to the Yagi-Uda loaded embedded plasmonic waveguide platform, leading a path toward highly integrated, spectrally functional plasmonic chips like resonant-guided wave networks²⁹ or on-chip detectors,¹² ideally with no need for subsequent intersections^{5,7,8} between different types of waveguides.

■ ASSOCIATED CONTENT

S Supporting Information

Experimental details on the fabrication, the farfield optical IR setup and characterization procedures, leakage microscopy measurements, spectral switching, NSOM measurements, experimental data analysis and statistics on the antennas, and directional couplers and numeric details on the FDTD simulations. This material is available free of charge via the Internet at <http://pubs.acs.org>.

■ AUTHOR INFORMATION

Corresponding Author

*E-mail: arian.kriesch@mpl.mpg.de.

Author Contributions

A.K. and S.P.B. conceived the experiments and developed the device design, A.K. performed numerical simulations and S.P.B. fabricated the samples. A.K., D.P., H.P., and S.P.B. performed the optical and FIB/SEM measurements. A.K., S.P.B., U.P., and H.A.A. analyzed the data and wrote the first draft of the

manuscript. All authors contributed to the final version of the manuscript.

Notes

The authors declare no competing financial interest.

ACKNOWLEDGMENTS

The authors thank P. Banzer, T. Bauer, S. Dobmann, J. S. Fakonas, and H. W. Lee for inspiring discussions and help with a new optical setup. This work was supported by the Cluster of Excellence Engineering of Advanced Materials (EAM), Erlangen and the Multidisciplinary University Research Initiative Grant (Air Force Office of Scientific Research, FA9550-10-1-0264). A.K. and D.P. also acknowledge funding from the Erlangen Graduate School in Advanced Optical Technologies (SAOT) by the German Research Foundation (DFG) in the framework of the German excellence initiative, A.K. by Friedrich Naumann Foundation, and S.P.B. by the National Science Foundation. We acknowledge use of facilities of the Kavli Nanoscience Institute (KNI) at Caltech and the Max Planck Institute for the Science of Light (MPL), Erlangen.

REFERENCES

- (1) Engheta, N. *Science* **2007**, *317*, 1698–702.
- (2) Miller, D. A. B. *Proc. IEEE* **2009**, *97*, 1166–1185.
- (3) Zia, R.; Schuller, J. A.; Chandran, A.; Brongersma, M. L. *Mater. Today* **2006**, *9*, 20–27.
- (4) Gramotnev, D. K.; Bozhevolnyi, S. I. *Nat. Photonics* **2010**, *4*, 83–91.
- (5) Delacour, C.; Blaize, S.; Grosse, P.; Fedeli, J. M.; Bruyant, A.; Salas-Montiel, R.; Lerondel, G.; Chelnokov, A. *Nano Lett.* **2010**, *10*, 2922–6.
- (6) Asghari, M.; Krishnamoorthy, A. V. *Nat. Photonics* **2011**, *5*, 268–270.
- (7) Gosciniak, J.; Volkov, V. S.; Bozhevolnyi, S. I.; Markey, L.; Massenot, S.; Dereux, A. *Opt. Express* **2010**, *18*, 5314–9.
- (8) Briggs, R. M.; Grandidier, J.; Burgos, S. P.; Feigenbaum, E.; Atwater, H. A. *Nano Lett.* **2010**, *10*, 4851–4857.
- (9) Uda, S. *Proc. IRE* **1927**, *15*, 377–385.
- (10) Yariv, A. *IEEE J. Quantum Electron.* **1973**, *9*, 919–933.
- (11) Alferness, R. C. *Science* **1986**, *234*, 825–829.
- (12) Ly-Gagnon, D.-S.; Balram, K. C.; White, J. S.; Wahl, P.; Brongersma, M. L.; Miller, D. A. B. *Nanophotonics* **2012**, *1*.
- (13) Cai, W.; Shin, W.; Fan, S.; Brongersma, M. L. *Adv. Mater.* **2010**, *22*, 5120–5124.
- (14) Berini, P.; De Leon, I. *Nat. Photonics* **2011**, *6*, 16–24.
- (15) Banzer, P.; Peschel, U.; Quabis, S.; Leuchs, G. *Opt. Express* **2010**, *18*, 10905–10923.
- (16) Novotny, L.; van Hulst, N. *Nat. Photonics* **2011**, *5*, 83–90.
- (17) Biagioni, P.; Huang, J.-S.; Hecht, B. *Rep. Prog. Phys.* **2012**, *75*, 024402.
- (18) Wen, J.; Romanov, S.; Peschel, U. *Opt. Express* **2009**, *17*, 5925.
- (19) Wen, J.; Banzer, P.; Kriesch, A.; Ploss, D.; Schmauss, B.; Peschel, U. *Appl. Phys. Lett.* **2011**, *98*, 101109.
- (20) Novotny, L. *Phys. Rev. Lett.* **2007**, *98*.
- (21) Andryieuski, A.; Malureanu, R.; Biagi, G.; Holmgård, T.; Lavrinenko, A. *Opt. Lett.* **2012**, *37*, 1124–1126.
- (22) Coenen, T.; Vesseur, E. J. R.; Polman, A.; Koenderink, A. F. *Nano Lett.* **2011**, *11*, 3779–84.
- (23) Curto, A. G.; Volpe, G.; Tamini, T. H.; Kreuzer, M. P.; Quidant, R.; van Hulst, N. F. *Science* **2010**, *329*, 930–3.
- (24) Bernal Arango, F.; Kwadrin, A.; Koenderink, A. F. *ACS Nano* **2012**, *6*, 10156–67.
- (25) Dorfmüller, J.; Dregely, D.; Esslinger, M.; Khunsin, W.; Vogelgesang, R.; Kern, K.; Giessen, H. *Nano Lett.* **2011**, *11*, 2819–24.
- (26) Dionne, J. A.; Sweatlock, L. A.; Atwater, H. A.; Polman, A. *Phys. Rev. B* **2006**, *73*.
- (27) Trinh, P. D.; Yegnanarayanan, S.; Jalali, B. *Electron. Lett.* **1995**, *31*, 2097–2098.
- (28) Boltasseva, A.; Nikolajsen, T.; Leosson, K.; Kjaer, K.; Larsen, M. S.; Bozhevolnyi, S. I. *J. Lightwave Technol.* **2005**, *23*, 413–422.
- (29) Feigenbaum, E.; Burgos, S. P.; Atwater, H. A. *Opt. Express* **2010**, *18*, 25584–25595.